

Article

# Radio-, Thermo- and Photoluminescence Properties of Lu<sub>2</sub>O<sub>3</sub>:Eu and Lu<sub>2</sub>O<sub>3</sub>:Tb Nanopowder and Film Scintillators

P. Popielarski <sup>1</sup>, J. Zeler <sup>2</sup>, P. Bolek <sup>2</sup>, T. Zorenko <sup>1</sup>, K. Paprocki <sup>1</sup>, E. Zych <sup>2,\*</sup>  
and Yu. Zorenko <sup>1,\*</sup>

<sup>1</sup> Institute of Physics of Kazimierz Wielki University in Bydgoszcz, 85-090 Bydgoszcz, Poland; pawelpop@ukw.edu.pl (P.P.); tzorenko@ukw.edu.pl (T.Z.); paprocki@ukw.edu.pl (K.P.)

<sup>2</sup> Faculty of Chemistry, University of Wrocław, 50-383 Wrocław, Poland; justyna.zeler@chem.uni.wroc.pl (J.Z.); paulina.bolek@chem.uni.wroc.pl (P.B.)

\* Correspondence: eugeniusz.zych@chem.uni.wroc.pl (E.Z.); zorenko@ukw.edu.pl (Y.Z.)

Received: 22 February 2019; Accepted: 8 March 2019; Published: 13 March 2019



**Abstract:** This work is dedicated to the preparation and characterization of the radio-, thermo-, and photoluminescent properties of Lu<sub>2</sub>O<sub>3</sub>:Eu and Lu<sub>2</sub>O<sub>3</sub>:Tb nanopowder (NPs) scintillators, prepared by means of hydrothermal processing, and their film analogues made of these NPs by the spin coating method. The luminescent properties of NPs and films were characterized by cathodoluminescence (CL), photoluminescence (PL), X-ray excited radioluminescence (RL), and thermoluminescence (TL) at low and high temperatures. In Lu<sub>2</sub>O<sub>3</sub>:Eu NPs and films, mostly the luminescence of Eu<sup>3+</sup> ions occupying the C<sub>2</sub> site of the host, with the most intensive peaks at 611.6 nm and a decay time of 1.5 ms, was observed. On the contrary, two types of Tb<sup>3+</sup> centers in the C<sub>2</sub> and C<sub>3i</sub> sites with the main emission lines at 542.4 and 544.0 nm and the corresponding 4f→5d excitation bands at 270 and 305 nm and decay times of  $t_{1/e} = 2.17$  and 3.96 ms were observed in the case of Lu<sub>2</sub>O<sub>3</sub>:Tb NPs and films. Indications were noted that Tb<sup>3+</sup> in the C<sub>3i</sub> symmetry position was most active in the CL spectra of Lu<sub>2</sub>O<sub>3</sub>:Tb NPs and a respective film. Thermoluminescent peaks at 110 °C and 170 °C for Lu<sub>2</sub>O<sub>3</sub>:Eu NPs and at 75 °C and 120 °C in Lu<sub>2</sub>O<sub>3</sub>:Tb NPs were observed corresponding to the hole and electron traps, respectively. Significantly different onsets of temperature quenching of Eu<sup>3+</sup> and Tb<sup>3+</sup> luminescence in Lu<sub>2</sub>O<sub>3</sub>:Eu and Lu<sub>2</sub>O<sub>3</sub>:Tb NPs were found at ~90 °C and ~320 °C, respectively.

**Keywords:** Lu<sub>2</sub>O<sub>3</sub>; Eu<sup>3+</sup>; Tb<sup>3+</sup>; luminescence; nanopowders; films; spin coating

## 1. Introduction

Lu<sub>2</sub>O<sub>3</sub> (lutetia) is a structural analog of Y<sub>2</sub>O<sub>3</sub> sesquioxide. Both are well-known hosts for rare-earth doped phosphors and scintillators. Eu<sup>3+</sup> and Tb<sup>3+</sup> doped Lu<sub>2</sub>O<sub>3</sub> oxides are mostly researched as sintered ceramics and nanocrystalline powder (NP) X-ray phosphors [1–3]. Due to its extremely high density of 9.42 g/cm<sup>3</sup> (one of the densest inorganic compounds) and high effective Z-number  $Z_{\text{eff}} = 67.3$ , Lu<sub>2</sub>O<sub>3</sub>-based phosphors attract attention as film scintillating screens for 2D/3D microimaging using X-ray or synchrotron radiation [4,5]. However, the properties of these materials in the various crystalline forms were found to be influenced by the differences in the methods and conditions of their preparation [6]. Understanding of these dependencies is important for deliberate management of phosphors properties according to the application needs.

Apart from the liquid phase epitaxy (LPE), which enables receiving Lu<sub>2</sub>O<sub>3</sub>:Eu single crystalline films from a few to tens of microns thick [5,6], other methods of film preparation, such as magnetron sputtering [7], pulse laser depositing [8,9], spin coating [10,11], etc., can be utilized for the fabrication of films of reasonable thicknesses. Most interesting are the methods of Lu<sub>2</sub>O<sub>3</sub> film preparation, with

thicknesses in the range of tens of nm to one micron, e.g., in the range where LPE cannot be used. This can be realized in the case of film preparation from the respective  $\text{Lu}_2\text{O}_3$  based NPs using spin coating (SC) technology [10,11].

The aim of our work is the preparation and characterization of the luminescent properties of  $\text{Lu}_2\text{O}_3:\text{Eu}$  and  $\text{Lu}_2\text{O}_3:\text{Tb}$  NPs as well as their thin film counterparts with thicknesses in the submicron range, prepared by the SC method using the mentioned NPs. Such a study is especially important for producing scintillating screens for microimaging with high special resolution in the micron scale. For characterization of the luminescent properties of NP and films, data from complementary spectroscopic methods, such as cathodoluminescence, photoluminescence, radioluminescence, and thermoluminescence, were used.

## 2. Sample Preparation and Experimental Techniques

The  $\text{Lu}_2\text{O}_3:3\%\text{Eu}$  and  $\text{Lu}_2\text{O}_3:1\%\text{Tb}$  NPs were sintered by means of hydrothermal processing [2]. For preparation of these NP phosphors, appropriate amounts of  $\text{Lu}_2\text{O}_3$  and/or  $\text{Eu}_2\text{O}_3$  and  $\text{Tb}_4\text{O}_7$  oxides were dissolved in diluted  $\text{HNO}_3$  at 80 °C. Then solid KOH was added until pH = 12. The immediately-formed suspension was cooled to room temperature (RT) and poured into an autoclave with a Teflon liner. The autoclave was heated at 230 °C for 10 h. After cooling, the precipitate was separated and washed several times with a water–ethanol mixture and dried. Finally, the powder was heat-treated at 900 °C for 5 h and then for 2 h at 950 °C in air.

The  $\text{Lu}_2\text{O}_3:\text{Eu}$  and  $\text{Lu}_2\text{O}_3:\text{Tb}$  thin NP films were prepared on quartz substrates using the SC method. Zinc acetate 2-hydrate ( $\text{Zn}(\text{CH}_3\text{COO})_2 \cdot 2\text{H}_2\text{O}$ , 99.5%) was dissolved at RT in isopropanol. Afterwards the ethanolamine ( $\text{NH}_2\text{CH}_2\text{CH}_2\text{OH}$ , MEA 98.0%) was added to the solution as a sol stabilizer. The molar ratio of ethanolamine to zinc acetate in solution was adjusted to 1:1 and the concentration of zinc acetate was 1.0 mol/L. The prepared mixtures were stirred at 333 K using a magnetic stirrer for about 1 h to obtain a clear homogeneous solution. Then 0.003 g of  $\text{Lu}_2\text{O}_3:\text{Eu}$  or  $\text{Lu}_2\text{O}_3:\text{Tb}$  NPs was added to the respective solutions. The thin NP film was deposited onto quartz substrates by the SC method with a speed rotation of 2000 r/min for 20 s. Each coated layer was dried at 353 K for 30 min to evaporate the solvent. The thickness of each dry layer was about 50 nm. The process was repeated to obtain a desired thickness of films in the 100–300 nm range. Finally, the thin NP films were heated in ambient atmosphere at the temperature of 823K for 1 h [12,13].

A D8 Advance diffractometer from Bruker (Billerica, MA, USA) with  $\text{Cu K}_{\alpha 1}$  radiation of 1.54060 Å wavelength was used for X-ray diffractometry to determine the phase purity of samples. The morphology of the nanoparticles and films were studied using Hitachi S-3400N (Hitachi High-Technologies, Tokyo, Japan) and JEOL JSM 820 (JEOL, Tokyo, Japan) scanning electron microscopes, respectively. Cathodoluminescence (CL) spectra of  $\text{Lu}_2\text{O}_3:\text{Eu}$  and  $\text{Lu}_2\text{O}_3:\text{Tb}$  NPs and films with 1.0 nm resolution were measured at RT using the JEOL JSM-820 electron microscope, additionally equipped with a high-sensitivity spectrometer Steller Net Silver Nova with a grating monochromator, respective software, and an electronically-cooled CCD detector (StellarNet, Tampa, USA) working in the 200–1200 nm range. The photoluminescence (PL) emission and excitation spectra as well as PL decay kinetics of  $\text{Lu}_2\text{O}_3:\text{Eu}$  and  $\text{Lu}_2\text{O}_3:\text{Tb}$  NPs at RT were investigated using a FLS 980 Edinburgh Instruments spectrometer (Edinburgh Instruments Ltd., Livingston Scotland) Thermally stimulated luminescence (TSL) glow curves, TSL luminescence spectra, and radioluminescence (RL) spectra were recorded using a Lexsygresearch Fully Automated TL/OSL Reader from Freiberg Instruments GmbH, (Freiberg, Germany). The source of white X-rays was a Varian VF-50J RTG X-ray tube with a W-anode. The TSL glow curves were collected with a 9235QB-type photomultiplier from ET Enterprises (Uxbridge, UK). TSL emission spectra were recorded with an Andor DU420A-OE CCD camera and were not corrected for the system sensitivity. All modules were operated by means of LexStudio 2 software and resultant data were processed under LexEva 2 analytical software dedicated to the TL/OSL Reader and supplied by the manufacturer (Freiberg Instruments GmbH, Freiberg, Germany).

### 3. Structural and Morphological Properties of $\text{Lu}_2\text{O}_3\text{:Eu}$ and $\text{Lu}_2\text{O}_3\text{:Tb}$ NPs and Films

The structure and morphology of NPs and films were studied using X-ray diffraction (XRD) and scanning electron microscopy (SEM), respectively. Measured XRD patterns of the  $\text{Lu}_2\text{O}_3\text{:Eu}$  and  $\text{Lu}_2\text{O}_3\text{:Tb}$  powders are presented in Figure 1 together with a simulated pattern ICSD#40471 of  $\text{Lu}_2\text{O}_3$  [3]. Analogous data were collected for films. As expected, they did not differ from the powders despite small background from the amorphous substrate. Therefore they are not separately presented here.

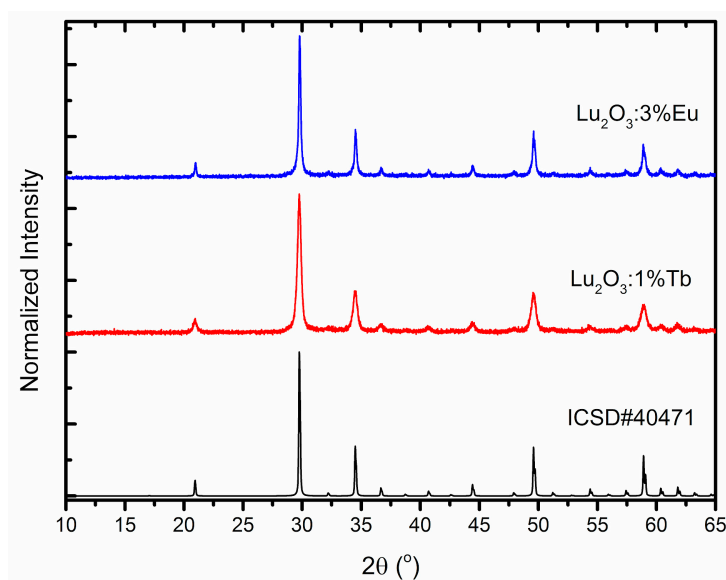


**Figure 1.** XRD patterns of the  $\text{Lu}_2\text{O}_3\text{:Eu}$  and  $\text{Lu}_2\text{O}_3\text{:Tb}$  powders and the simulated one for cubic  $\text{Lu}_2\text{O}_3$  [3].

It is clear that, to the level of the detection limit of the technique, no foreign phases were observed in any of the phosphors. In both cases the diffraction lines were broadened signifying that they were composed of nanosized crystallites which was proven by means of the high resolution SEM images presented below. Furthermore, no broad band underlying the regular XRD pattern was seen for any of the powders which implied that the amorphous fraction was not present or its amount was insignificant. This is advantageous for spectroscopic properties.

However, as shown in Figure 2, the morphology of the samples was noticeably different in the case of  $\text{Lu}_2\text{O}_3\text{:Eu}$  (Figure 2a) and  $\text{Lu}_2\text{O}_3\text{:Tb}$  (Figure 2b) powders despite the apparently identical conditions of preparation of the phosphors. Ball-like particles were formed in the case of  $\text{Lu}_2\text{O}_3\text{:Eu}$  whereas dendrite-like structures appeared in the case of  $\text{Lu}_2\text{O}_3\text{:Tb}$  (Figure 2a,b, respectively). The reasons for such a significant difference are not clear and will be further investigated. One can presume that the unavoidable presence of  $\text{Tb}^{4+}$  during the formation of the  $\text{Lu}_2\text{O}_3\text{:Tb}$  particles may play a crucial role here. The SEM images prove that both powders are nanocrystalline with crystallites smaller than 100 nm. Particles tended to agglomerate but no hard aggregates were exposed.

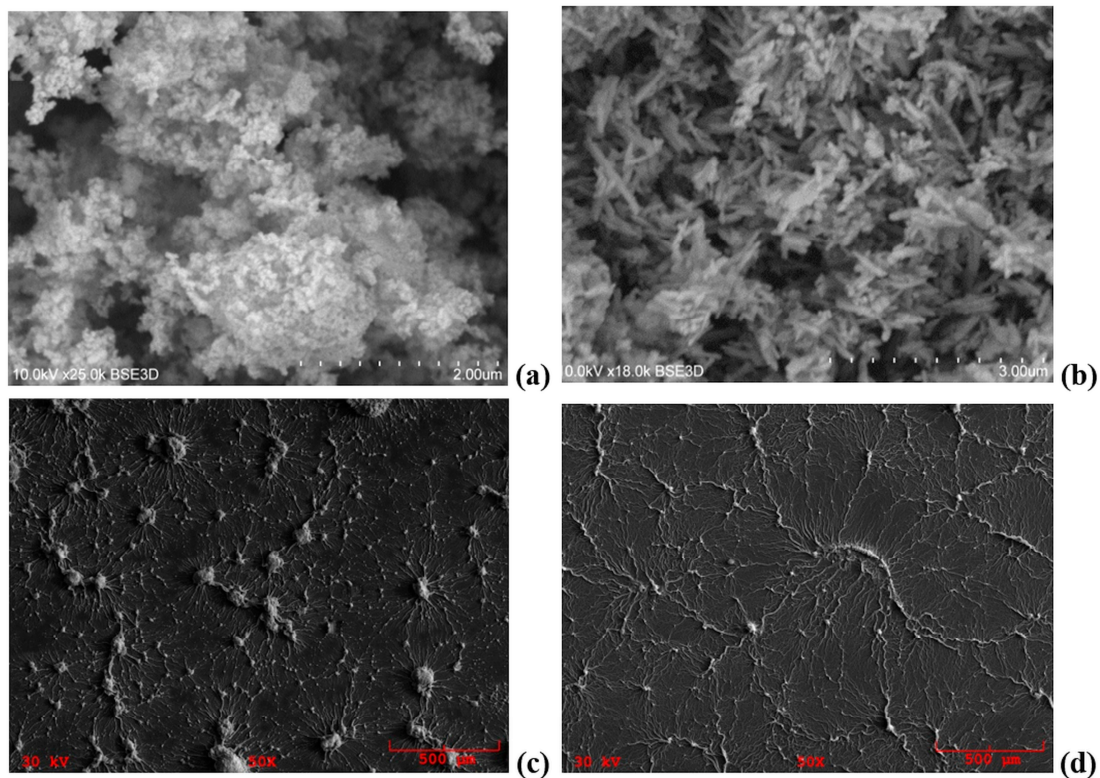


**Figure 2.** Morphology of  $\text{Lu}_2\text{O}_3:\text{Eu}$  (a) and  $\text{Lu}_2\text{O}_3:\text{Tb}$  (b) NPs as well as  $\text{Lu}_2\text{O}_3:\text{Eu}$  (c) and  $\text{Lu}_2\text{O}_3:\text{Tb}$  (d) films with thickness of about 300 nm.

The morphology of Eu- and Tb-doped  $\text{Lu}_2\text{O}_3$  films is shown in Figure 2c,d, respectively. The respective  $\text{Lu}_2\text{O}_3:\text{Eu}$  and  $\text{Lu}_2\text{O}_3:\text{Tb}$  NPs were embedded in the specific needle-like nets onto the quartz substrate surface. Thus, in the case of  $\text{Lu}_2\text{O}_3:\text{Tb}$ , more uniform phosphor was netted onto substrate surface with a small quantity of the large-dimensional conglomerates observed. For  $\text{Lu}_2\text{O}_3:\text{Eu}$  films, the quantity and size of such conglomerates were significantly larger. Apparently, differences in the morphology of  $\text{Lu}_2\text{O}_3:\text{Eu}$  and  $\text{Lu}_2\text{O}_3:\text{Tb}$  NPs (Figure 2a,b) led to the difference in the surface morphology of the respective films, formed by means of the SC method. In the future a significant effort should be made towards improvement of the film morphology.

The difference in the uniformity of the  $\text{Lu}_2\text{O}_3:\text{Eu}$  and  $\text{Lu}_2\text{O}_3:\text{Tb}$  NPs films was also confirmed by the respective absorption spectra of these films with thicknesses in the 100–300 nm range. Namely, the background level significantly increased with the thickness for  $\text{Lu}_2\text{O}_3:\text{Eu}$  films (Figure 3a) while in the case of  $\text{Lu}_2\text{O}_3:\text{Tb}$  films, only insignificant differences were seen (Figure 3b). It is thus expected that optimization of film fabrication (necessarily combined with optimization of the NPs preparation) may create high levels of film uniformity and consequently homogeneity of their spectroscopic properties.

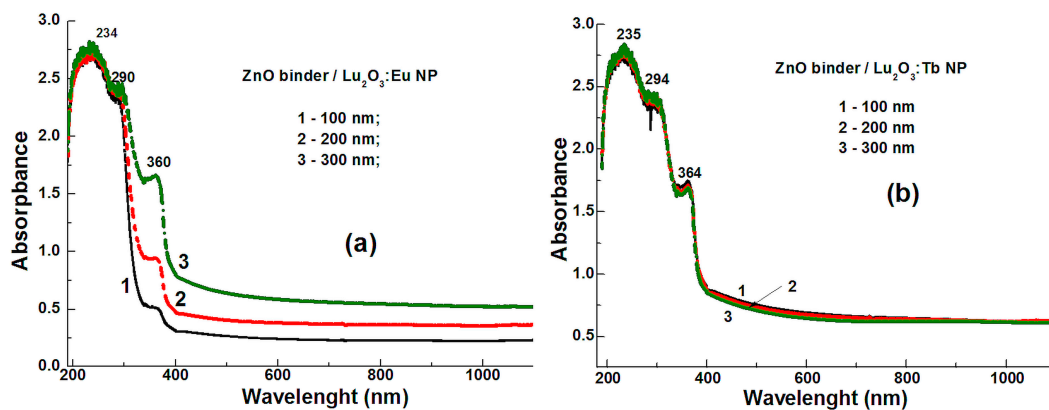


**Figure 3.** Absorption spectra of  $\text{Lu}_2\text{O}_3:\text{Eu}$  (a) and  $\text{Lu}_2\text{O}_3:\text{Tb}$  (b) films with thicknesses of about of 100 nm (1), 200 nm (2), and 300 nm (3). Due to the close shape of the absorption spectra of  $\text{Lu}_2\text{O}_3:\text{Eu}$  (a) and  $\text{Lu}_2\text{O}_3:\text{Tb}$  (b) films, the bands peaked at 360–364 nm, 290–294 nm, and 234–235 nm ranges which rather corresponded to the absorption of the ZnO based binder and was not related to the absorption of the NP films due to their very low thickness in the 100–300 nm range.

#### 4. Luminescent Properties of $\text{Lu}_2\text{O}_3:\text{Eu}$ and $\text{Lu}_2\text{O}_3:\text{Tb}$ NPs and Films

The  $\text{Lu}_2\text{O}_3$  lattice provides two positions with different symmetry of  $\text{Lu}^{3+}$  cations and consequently also of the  $\text{Eu}^{3+}$  and  $\text{Tb}^{3+}$  dopants [3]. These are centrosymmetric  $C_{3i}$  (often termed  $S_6$  in the spectroscopic literature which is not fully correct) and lower-symmetry non-centrosymmetric  $C_2$  sites. The population of the latter is triple the population of the former. Generally speaking, for the  $C_{3i}$  sites the electric dipole  $4f-4f$  transitions are forbidden and emission spectra of the  $\text{Lu}_2\text{O}_3:\text{Eu}$  and  $\text{Lu}_2\text{O}_3:\text{Tb}$  NPs are dominated by transitions of  $\text{Eu}^{3+}$  and  $\text{Tb}^{3+}$  ions occupying the  $C_2$  sites [2,3] unless direct selective excitation into the dopant in the  $C_{3i}$  site is applied. Furthermore, at least for the  $\text{Eu}^{3+}$  activator, significant  $\text{Eu}(C_{3i}) \rightarrow \text{Eu}(C_2)$  energy transfer occurs when the dopant content increases above  $\sim 1$  mol% [2].

It was proven that the  $\text{Eu}^{3+}$  and  $\text{Tb}^{3+}$  luminescence can be different in the various  $\text{Lu}_2\text{O}_3$  crystalline forms (single crystals, powders, films) [6]. This was attributed mainly to a different concentration of oxygen vacancies which interfere with the host–activator energy transfer under excitation above the  $\text{Lu}_2\text{O}_3$  host band gap in the different crystalline  $\text{Lu}_2\text{O}_3$  samples [6].

The luminescent properties of  $\text{Lu}_2\text{O}_3:\text{Eu}$  NPs and  $\text{Lu}_2\text{O}_3:\text{Tb}$  NPs were characterized by cathodoluminescence (CL), X-ray excited radioluminescence (RL), photoluminescence (PL), and thermoluminescence (TSL) measurements in a broad range of temperatures, both below and above room temperature. Due to the very low thicknesses of the  $\text{Lu}_2\text{O}_3:\text{Eu}$  NP films (100–300 nm) their RL and TSL properties could not be effectively investigated.

##### 4.1. $\text{Lu}_2\text{O}_3:\text{Eu}$ NPs and Films

**Cathodoluminescence:** The CL spectra of both  $\text{Lu}_2\text{O}_3:\text{Eu}$  NPs and films showed quite similar shapes (Figure 3). The most intensive CL emission peak was observed at 612 nm, which corresponded to the  ${}^5\text{D}_0 \rightarrow {}^7\text{F}_2$  transitions of  $\text{Eu}^{3+}$  ions in the  $C_2$  site. In both spectra some contribution from the  ${}^5\text{D}_0 \rightarrow {}^7\text{F}_0$  transitions as well as the low-intensity  ${}^5\text{D}_0 \rightarrow {}^7\text{F}_1$  transitions of  $\text{Eu}^{3+}$  ions was also observed. According to literature, in this range there might also be some light generated by the  $\text{Eu}^{3+}$  occupying the  $C_{3i}$  site [2]. It is noteworthy that some contribution from the  ${}^5\text{D}_1$  level in the  $\sim 525\text{--}570$  nm range of wavelengths was also evident in the CL spectra of  $\text{Lu}_2\text{O}_3:\text{Eu}$  NP (Figures 3 and 4).

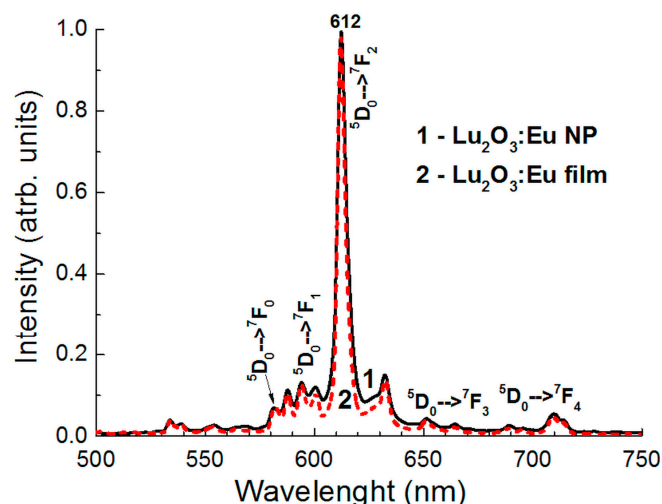


**Figure 4.** Cathodoluminescence (CL) spectra of  $\text{Lu}_2\text{O}_3:\text{Eu}$  nanopowder (NP) (1) and film (2) samples at room temperature (RT).

**Photoluminescence:** The PL emission spectra of  $\text{Lu}_2\text{O}_3:\text{Eu}$  NPs at RT were quite similar at different excitation energies and consisted of a group of strong lines caused by the  $^5\text{D}_0 \rightarrow ^7\text{F}_j$  ( $j = 0-4$ ) transitions of  $\text{Eu}^{3+}$  ions (Figure 5a,b). The most intensive emission peak was observed at 611.6 nm (Figure 5a, curve 1) which corresponded to the  $^5\text{D}_0 \rightarrow ^7\text{F}_2$  transition of  $\text{Eu}^{3+}$  ions in the  $\text{C}_2$  site. The  $^5\text{D}_0 \rightarrow ^7\text{F}_0$  transition of  $\text{Eu}^{3+}$  ions in the  $\text{C}_2$  sites at 580.5 nm was clearly observed in the PL spectra of  $\text{Lu}_2\text{O}_3:\text{Eu}$  NPs (Figure 5b). That indirectly confirmed the very good quality of the phosphor [8]. No emission of  $\text{Eu}^{2+}$  ions was detected in the  $\text{Lu}_2\text{O}_3:\text{Eu}$  NPs. As is presented in Figure 5c, the main luminescent line showed basically exponential decay with the time constant  $\tau = 1.5$  ms. This was noticeably longer than in the case of coarse grains of the same composition, when the decay was about 1.0 ms [14]. The elongation of the decay time in nanopowders was described and explained first by Meltzer [15,16]. Good quality NPs show longer decay times than their micron-sized counterparts because the effective refractive index  $n$  felt by the emitting ion in nanopowders is significantly lower than in the coarse-grained materials [14–18]. In the latter, the refractive index  $n$  is defined by the host, while in the former, air (vacuum) contributes to the effective  $n$  value. The exponential, and much longer than in crystals, decay of  $\text{Eu}^{3+}$  luminescence in the  $\text{Lu}_2\text{O}_3:\text{Eu}$  NPs prove their high quality and low population of defects.

The excitation spectrum of the  $\text{Eu}^{3+}$  611.6 nm luminescence ( $\text{C}_2$  site) of  $\text{Lu}_2\text{O}_3:\text{Eu}$  NP (Figure 5a, curve 2) consisted of sharp lines in the 270–550 nm range, corresponding to the intrinsic  $4f \rightarrow 4f$  transitions of  $\text{Eu}^{3+}$  ions. Narrow, well-resolved excitation lines again attested to the high structural quality of the fabricated  $\text{Lu}_2\text{O}_3:\text{Eu}$  NPs. A strong wide excitation band peaking at approximately 260 nm was related to the  $\text{O}^{2-} \rightarrow \text{Eu}^{3+}$  charge transfer transitions (CTT). One might be surprised by the high intensity of the  $4f \rightarrow 4f$  excitation transitions of  $\text{Eu}^{3+}$  compared to its CTT band. This was already explained years ago [19] for  $\text{Lu}_2\text{O}_3:\text{Eu}$  and even earlier [20] for electronic and vibronic transitions of  $\text{Pr}^{3+}$  in other compositions as resulting from the saturation effect which effectively suppresses the measured intensity of the CCT. This occurs because the very high absorption co-efficient of the charge transfer transitions precludes excitation of the whole depth of the phosphor layer, while much lower absorptivity due to  $4f \rightarrow 4f$  transitions allows the deeper penetration of the sample by radiation in the area of their occurrence.

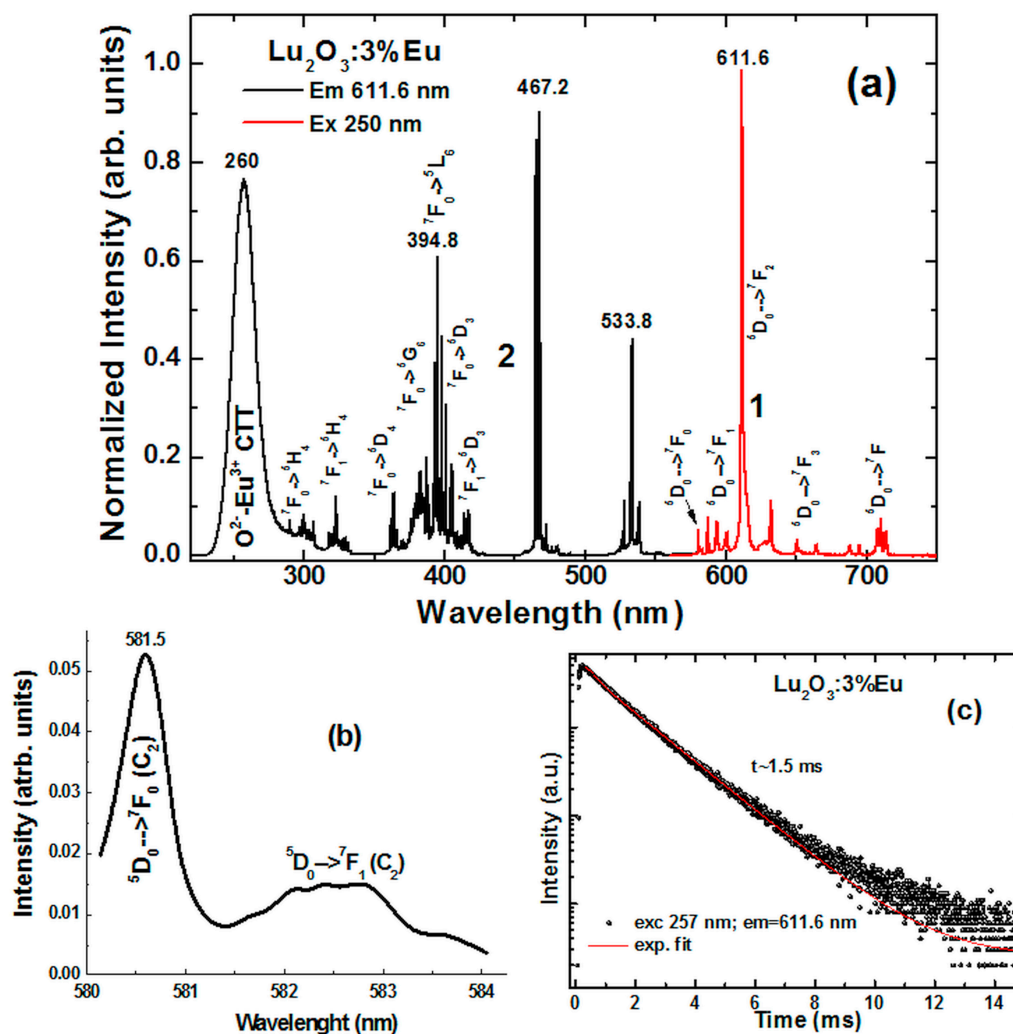


**Figure 5.** RT photoluminescence (PL) emission (1a, b) and excitation (2a) spectra (a) of  $\text{Eu}^{3+}$  luminescence as well as PL decay kinetic (c) of  $\text{Lu}_2\text{O}_3:\text{Eu}$  NP. (b) More detailed fragment of the excitation spectrum of  $\text{Eu}^{3+}$  luminescence in the 580–584 nm range related to the  $^5\text{D}_0 \rightarrow ^7\text{F}_{0,1}$  transitions.

**Thermally stimulated luminescence:** The TSL glow curve and evolution of TSL emission spectra of  $\text{Lu}_2\text{O}_3:\text{Eu}$  NPs with temperature are shown in Figure 6a,b, respectively. The positions of the main TSL peaks are located at  $\sim 110^\circ\text{C}$  and  $170^\circ\text{C}$  (Figure 6a). Already at room temperature some afterglow of  $\text{Lu}_2\text{O}_3:\text{Eu}$  NP was observed. The TSL emission spectra of  $\text{Lu}_2\text{O}_3:\text{Eu}$  NP were composed of  $\text{Eu}^{3+}$  luminescence exclusively (Figure 6b). According to the model of TSL processes [21–23],  $\text{Eu}^{3+}$  ions serve as electron traps, while the hole trap is expected to be connected with an intrinsic defect of the host. The relative intensity of the orange features of  $\text{Eu}^{3+}$  luminescence ( $\sim 585\text{--}600$  nm) in the TSL spectra (Figure 6b) was notably higher than in CL or PL spectra, presented in Figures 4 and 5. This indicated that  $\text{Eu}^{3+}$  ions in the  $\text{C}_{3i}$  site were more susceptible for trapping electrons than those in the  $\text{C}_2$  site and consequently more profoundly contribute to TSL. Such an observation was already reported in  $\text{Lu}_2\text{O}_3:\text{Eu}$  sintered ceramics [24]. Yet, in the ceramics it was observed only for lower concentrations of Eu, up to 1%, while here it was still seen for the Eu content of 3%. This size-effect should be a subject of more comprehensive and focused investigation in the future. Note that two spikes at  $\sim 650$  nm and  $\sim 730$  nm around  $260\text{--}270^\circ\text{C}$  seen in Figure 6b were artifacts resulting from an electronic noise of CCD used in this experiment.

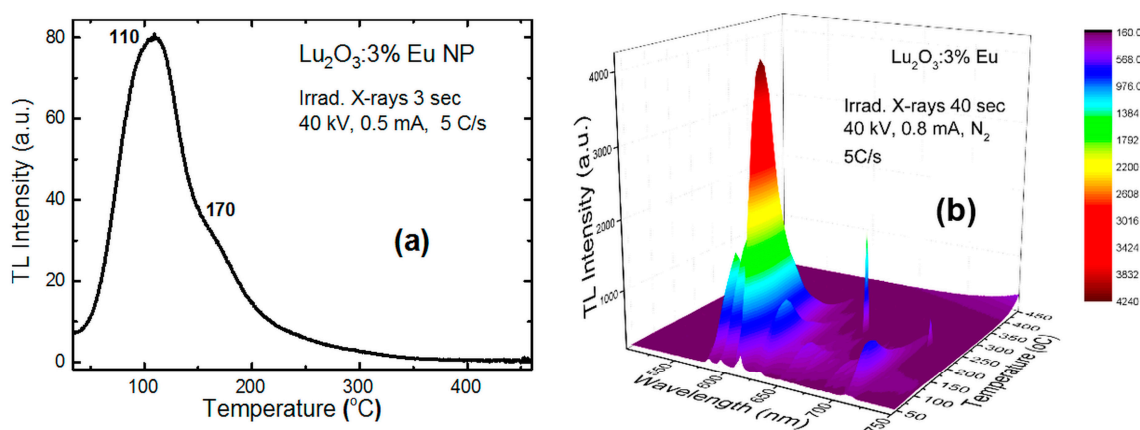


**Figure 6.** Thermally stimulated luminescence (TSL) glow curve (a) and TSL emission spectra (b) of Lu<sub>2</sub>O<sub>3</sub>:Eu NP after irradiation by X-ray at 300 K. The two spikes at ~650 nm and 730 nm around 260–270 °C in (b) are artifacts due to an electronic noise of CCD.

**Radioluminescence:** X-ray excited RL spectra of Lu<sub>2</sub>O<sub>3</sub>:Eu NPs were measured in the temperature range of 300–550 °C and the data are presented in Figure 7. Note how much less intense the relative intensity of the orange part (~585–600 nm) was in RL than it was in TSL (Figure 6b). Surprisingly, the maximum of RL intensity Lu<sub>2</sub>O<sub>3</sub>:Eu NP was observed around 320–330 °C. Hence, the overall efficiency of the RL was higher when temperature was well above the main TSL peaks (Figure 6). Therefore, this phenomenon had to be caused by a higher efficiency of energy transfer from the excited host to the dopant at such high temperatures. This, in turn, might imply that the light yield under X-ray reported in the past [1] might not reflect the real potential of this X-ray phosphor. This is a truly intriguing conclusion and this effect is worth much deeper investigation, and it is especially interesting that such results can be compared for different Eu concentrations.

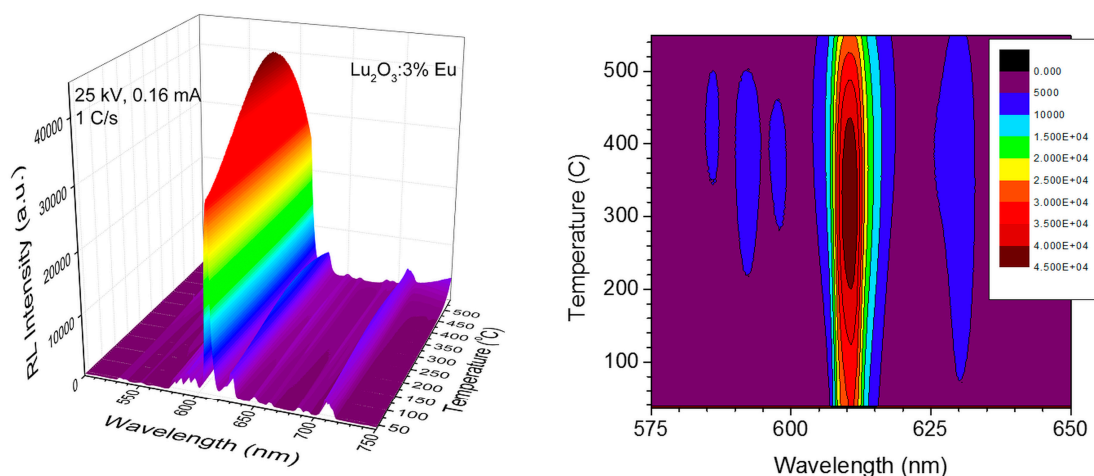


**Figure 7.** Temperature dependence of X-ray excited radioluminescence (RL) in Lu<sub>2</sub>O<sub>3</sub>:Eu NP in the 30–500 K range.

#### 4.2. Lu<sub>2</sub>O<sub>3</sub>:Tb NPs and films

**Cathodoluminescence:** The CL spectra of Lu<sub>2</sub>O<sub>3</sub>:Tb NPs and films were very similar (Figure 8). The most intensive emission peaks were observed at 543.5 and 552.2 nm, which upon site selective PL spectroscopy could be attributed to the <sup>5</sup>D<sub>4</sub>→<sup>7</sup>F<sub>j</sub> transitions of Tb<sup>3+</sup> ions in the Lu<sub>2</sub>O<sub>3</sub> host (Figure 9). Taking into account the spectral position of these bands in the PL spectra (Figure 9), the contribution of Tb<sup>3+</sup> luminescence in C<sub>3i</sub> centers may appear significant compared to C<sub>2</sub> centers in the CL spectra of

Lu<sub>2</sub>O<sub>3</sub>:Tb NPs and film. However, at present this is merely a supposition needing precise verification. Determination of a dominant type of emission center and estimation of the relative quantity of Tb<sup>3+</sup>(C<sub>2</sub>) and Tb<sup>3+</sup>(C<sub>3i</sub>) centers requires CL spectra recorded with a resolution much higher than 1 nm. This observation will be further verified and investigated in other crystalline forms of Lu<sub>2</sub>O<sub>3</sub>:Tb samples.

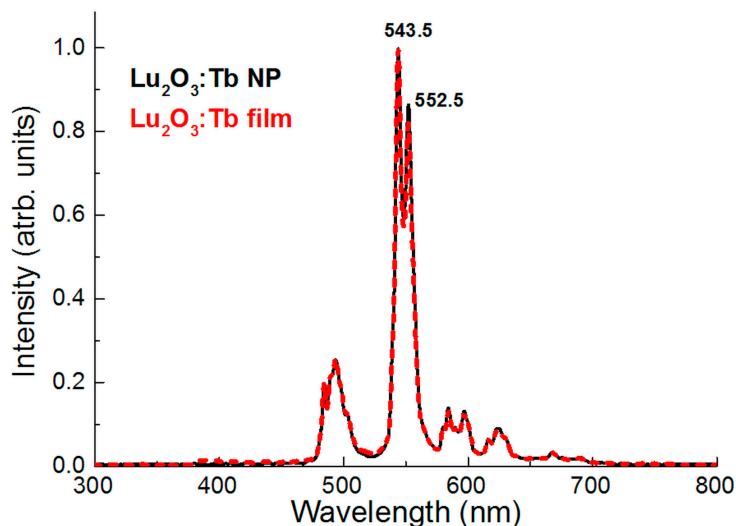


Figure 8. RT CL spectra of Lu<sub>2</sub>O<sub>3</sub>:Tb NP and film.

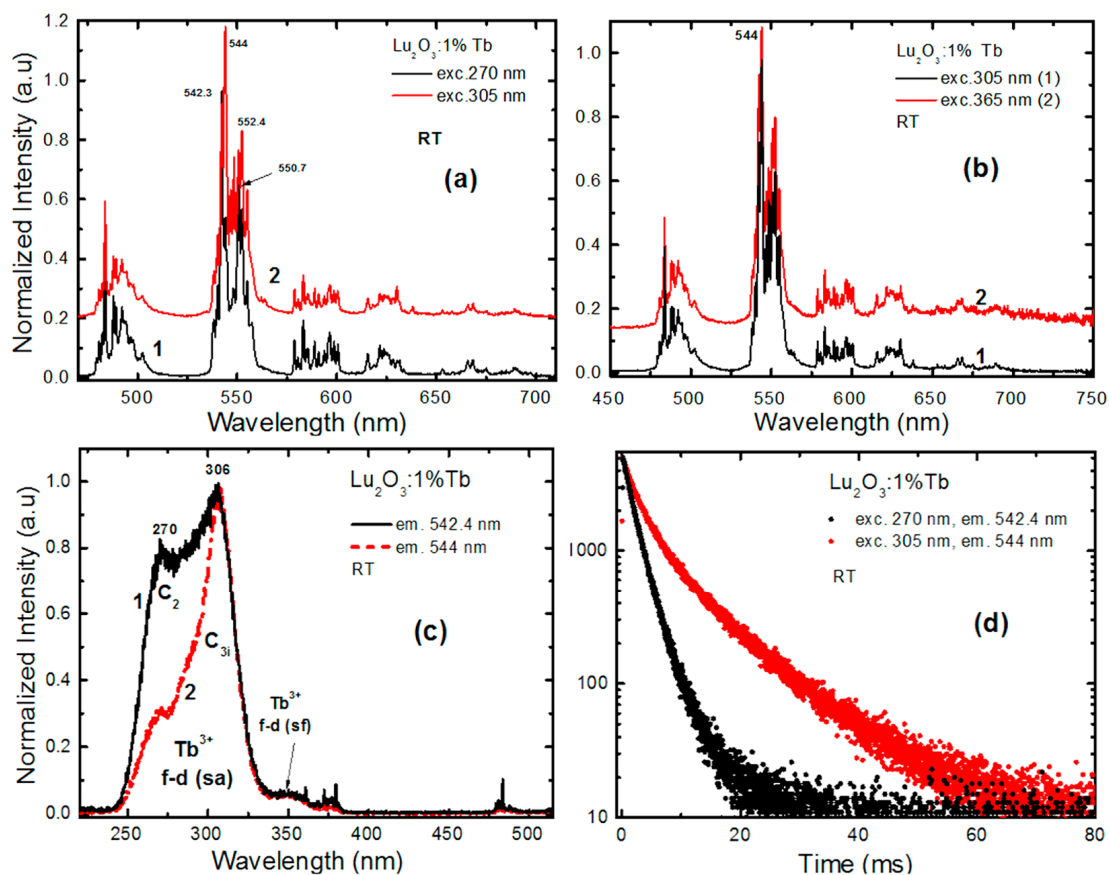
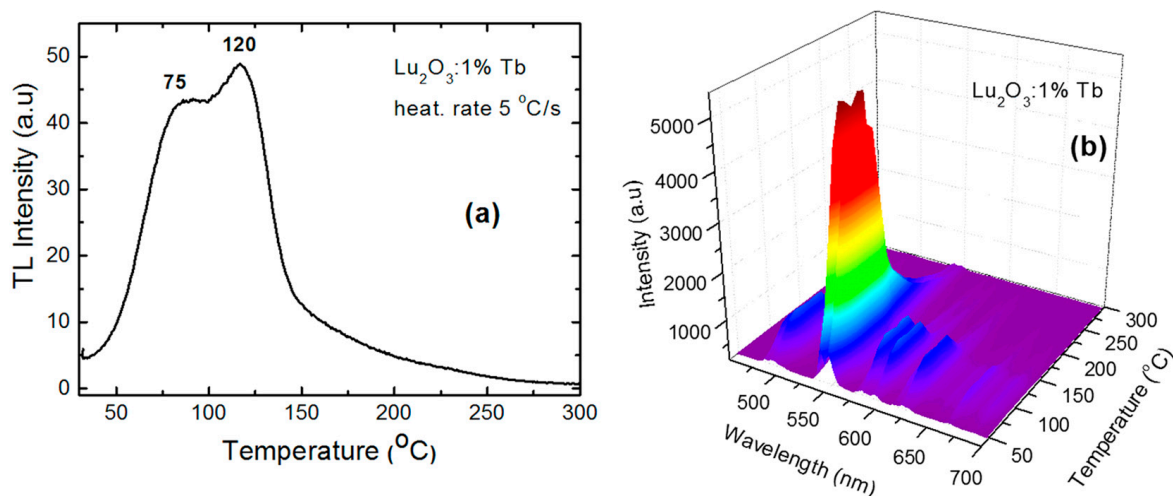


Figure 9. PL emission (a, b) and excitation spectra (c) as well as the PL decay kinetic (d) of Tb<sup>3+</sup> luminescence in Lu<sub>2</sub>O<sub>3</sub>:Tb NP at 300 K.

Photoluminescence: Contrary to the CL spectra, emissions from the two sites were clearly observed in the PL spectra of Lu<sub>2</sub>O<sub>3</sub>:Tb NP. Namely, the PL spectra of Tb<sup>3+</sup> ions in the C<sub>2</sub> and C<sub>3i</sub> positions possessed the main peaks at 542.4 and 544.0 nm, respectively (Figure 9a,b). Their excitation spectra also showed some differences, proving the presence of the two mentioned Tb<sup>3+</sup> sites (Figure 9c). Namely, the main excitation 4f→5d bands peaked at 270 nm for the C<sub>2</sub> site and at 306 nm for the C<sub>3i</sub> site of Tb<sup>3+</sup> in the Lu<sub>2</sub>O<sub>3</sub> host. A low-intensity excitation band around 365 nm was also observed in the PL excitation spectra and was proven to result from the spin-forbidden (sf) 4f→5d transitions of Tb<sup>3+</sup> ions both in C<sub>3i</sub> sites (Figure 9c). Therefore, excitation at 305 nm and 365 nm results in very similar PL spectra of Lu<sub>2</sub>O<sub>3</sub>:Tb NPs due to transitions within the Tb<sup>3+</sup> (C<sub>3i</sub>) (Figure 9a,b).

As expected, the decay kinetics of Tb<sup>3+</sup> luminescence deviate from the exponential course, especially for the C<sub>3i</sub> site. The latter was much longer than that of the C<sub>2</sub> sites (Figure 9d). For this reason, for decay curve characterization we have used the two decay times of  $\tau_{1/e} = 2.17$  ms and  $\tau_{1/20} = 3.96$  ms for Tb in C<sub>2</sub> and  $\tau_{1/e} = 7.32$  ms and  $\tau_{1/20} = 19.36$  ms for Tb in the C<sub>3i</sub> site of the Lu<sub>2</sub>O<sub>3</sub> host. As usual, there was a longer emission of ions in the site with inversion symmetry.

Thermally stimulated luminescence: An easily recordable but not very intense afterglow was observed in Lu<sub>2</sub>O<sub>3</sub>:Tb NPs at RT (Figure 10). The TSL glow curve was composed of two superimposed peaks with maxima around 75 °C and 120 °C. The TL emission spectrum was exclusively generated by Tb<sup>3+</sup> transitions. Due to the fact that Tb<sup>3+</sup> ions typically serve as hole traps, and because it was Tb<sup>3+</sup> which finally produced the TSL photons, the observed TSL peaks in Lu<sub>2</sub>O<sub>3</sub>:Tb NPs had to correspond to intrinsic electron trapping centers. These may result from oxygen vacancies. Similarly positioned TL peaks were reported for Lu<sub>2</sub>O<sub>3</sub>:Tb, Ca ceramics sintered at 1700 °C in a reducing atmosphere, where the oxygen vacancies were responsible for a very intense TL [25,26].



**Figure 10.** Glow curve (a) and TSL spectra (b) of Lu<sub>2</sub>O<sub>3</sub>:Tb NPs after irradiation with X-rays at 300 K.

Radioluminescence: The temperature dependence of the RL spectra of Lu<sub>2</sub>O<sub>3</sub>:Tb NPs was measured up to 500 °C (Figure 11). As can be seen from this figure, the Tb<sup>3+</sup> luminescence disappeared at about 400 °C. This resulted from a thermal quenching which was reported for Lu<sub>2</sub>O<sub>3</sub>:Tb sintered ceramics to start right at room temperature [27]. Note that in this experiment, the dependence of RL intensity on temperature was to some extent distorted by the appearance of TL photons which contributed quite significantly in the range of ~50–150 K (see Figure 10a).

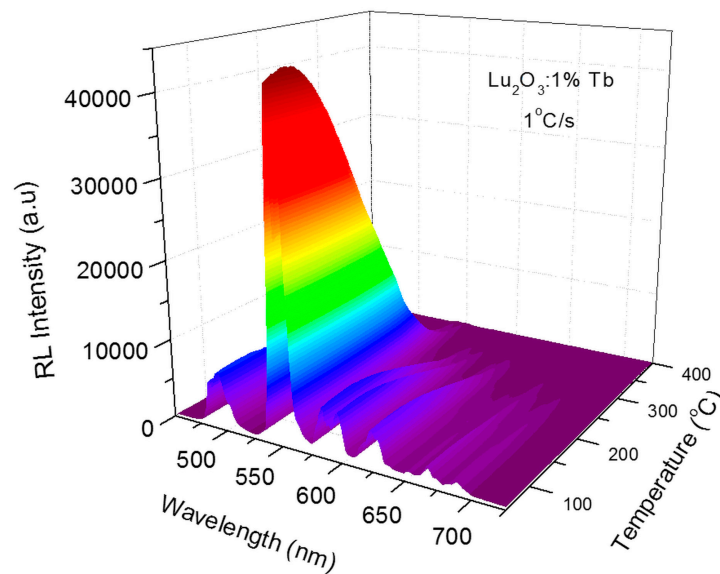


Figure 11. Temperature dependence of RL spectra of  $\text{Lu}_2\text{O}_3:\text{Tb}$  NP.

## 5. Conclusions

The  $\text{Lu}_2\text{O}_3:\text{Eu}$  and  $\text{Lu}_2\text{O}_3:\text{Tb}$  NPs were fabricated by means of hydrothermal processing. From the respective NPs the  $\text{Lu}_2\text{O}_3:\text{Eu}$  and  $\text{Lu}_2\text{O}_3:\text{Tb}$  thin films (from 100 up to 300 nm thick) were prepared using a spin-coating method. Despite undergoing essentially the same method of preparation, different morphology of  $\text{Lu}_2\text{O}_3:\text{Eu}$  and  $\text{Lu}_2\text{O}_3:\text{Tb}$  NPs was observed: ball-like particles were formed in the case of  $\text{Lu}_2\text{O}_3:\text{Eu}$  and dendrite-like structures in the case of  $\text{Lu}_2\text{O}_3:\text{Tb}$ . The morphological differences of powders resulted in differences of the morphology and structural quality of the respective films. Accordingly, the  $\text{Lu}_2\text{O}_3:\text{Tb}$  films possessed a more uniform surface than  $\text{Lu}_2\text{O}_3:\text{Eu}$  counterparts.

It was found that the CL and PL emission spectra as well as PL decay kinetic of  $\text{Lu}_2\text{O}_3:\text{Eu}$  NP and films showed the luminescence of  $\text{Eu}^{3+}$  ions almost exclusively from the  $\text{C}_2$  site of  $\text{Lu}_2\text{O}_3$  host with the most intensive peak at 611.6 nm and the decay time of about 1.5 ms, about 50% longer than in coarse grained ceramics.

Contrary to  $\text{Lu}_2\text{O}_3:\text{Eu}$ , the PL emission and excitation spectra as well as PL decay kinetic of  $\text{Lu}_2\text{O}_3:\text{Tb}$  NPs and films at 300 K showed two types of  $\text{Tb}^{3+}$  luminescence centers in the  $\text{C}_2$  and  $\text{C}_{3i}$  sites of the  $\text{Lu}_2\text{O}_3$  host with the main emission peaks at 542.4 and 544.0 nm and corresponding maxima of excitation bands located at 270 and 305 nm due to the  $4f \rightarrow 5d$  transition. The luminescence decay traces of  $\text{Tb}^{3+}$  ions in  $\text{C}_2$  and  $\text{C}_{3i}$  sites were non-exponential, especially for  $\text{Tb}^{3+}$  in the  $\text{C}_{3i}$  position, and the decay times of the  $\text{Tb}^{3+}(\text{C}_2)$  and  $\text{Tb}^{3+}(\text{C}_{3i})$  centers luminescence were equal to  $t_{1/e} = 2.17$  and  $t_{1/20} = 3.96$  ms and  $t_{1/20} = 7.32$  and  $t_{1/e} = 19.36$  ms, respectively.

The TL peaks at 110 °C and 170 °C and at 75 °C and 120 °C were observed in  $\text{Lu}_2\text{O}_3:\text{Eu}$  and  $\text{Lu}_2\text{O}_3:\text{Tb}$  NPs, respectively. They corresponded to the formation of the hole and electron trapping centers in the  $\text{Lu}_2\text{O}_3$  host, respectively. Significantly different temperature dependences of X-ray excited luminescence in  $\text{Lu}_2\text{O}_3:\text{Eu}$  and  $\text{Lu}_2\text{O}_3:\text{Tb}$  NPs was also evident. Namely, the start of the temperature quenching of  $\text{Eu}^{3+}$  and  $\text{Tb}^{3+}$  luminescence in  $\text{Lu}_2\text{O}_3:\text{Eu}$  and  $\text{Lu}_2\text{O}_3:\text{Tb}$  NPs was observed at 90 °C and 320 °C, respectively.

**Author Contributions:** P.P. performed preparation of NP film, T.Z. performed the measurement of their absorption spectra, K.P. performed the measurements of CL spectra of NP and film samples as well as the investigation of the morphology of films, Y.Z. analyzed the whole experimental materials and contributed in writing Introduction, NP film growth part, Experimental part and Conclusions of the paper. J.Z. synthesized nanocrystalline powders of  $\text{Lu}_2\text{O}_3:\text{Eu}$ , measured their XRD diffractograms, SEM images and performed PL, RL and TL experiments on them. P.B. synthesized nanocrystalline powders of  $\text{Lu}_2\text{O}_3:\text{Tb}$ , measured their XRD diffractograms and performed PL, RL and TL experiments on them. E.Z. contributed to experimental data analysis and writing the paper.

**Acknowledgments:** The work was performed in the frame of Polish National Science Centre (NCN) grants No 2016/21/B/ST8/03200 (Y.Z.) and No 2014/13/B/ST5/01535 (E.Z.).

**Conflicts of Interest:** The authors declare no conflict of interest.

## References

1. Lempicki, A.; Brecher, C.; Szupryczynski, P.; Lingertat, H.; Nagarkar, V.; Tipnis, S.; Miller, S. A new lutetia-based ceramic scintillator for X-ray imaging. *Nucl. Instrum. Methods Phys. Res. Sect. A Accel. Spectrometersdetectors Assoc. Equip.* **2002**, *488*, 579–590. [[CrossRef](#)]
2. Zych, E. Concentration dependence of energy transfer between  $\text{Eu}^{3+}$  ions occupying two symmetry sites in  $\text{Lu}_2\text{O}_3$ . *J. Phys. Condens. Matter* **2002**, *14*, 5637. [[CrossRef](#)]
3. Zeler, J.; Jerzykiewicz, L.B.; Zych, E. Flux-aided synthesis of  $\text{Lu}_2\text{O}_3$  and  $\text{Lu}_2\text{O}_3$ : Eu—single crystal structure, morphology control and radioluminescence efficiency. *Materials* **2014**, *7*, 7059–7072. [[CrossRef](#)]
4. Sengupta, D.; Miller, S.; Marton, Z.; Chin, F.; Nagarkar, V.; Prax, G. Bright  $\text{Lu}_2\text{O}_3$ : Eu thin-film scintillators for high-resolution radioluminescence microscopy. *Adv. Healthc. Mater.* **2015**, *4*, 2064–2070. [[CrossRef](#)] [[PubMed](#)]
5. Riva, F.; Martin, T.; Douissard, P.; Dujardin, C. Single crystal lutetium oxide thin film scintillators for X-ray imaging. *J. Instrum.* **2016**, *11*, C10010. [[CrossRef](#)]
6. Zorenko, T.; Gorbenko, V.; Safronova, N.; Matveevskaya, N.; Yavetskiy, R.; Babayevska, N.; Zorenko, Y. Comparative study of the luminescent properties of oxide compounds under synchrotron radiation excitation:  $\text{Lu}_2\text{O}_3$ : Eu nanopowders, ceramics and films. *J. Lumin.* **2018**, *199*, 461–464. [[CrossRef](#)]
7. Bellocchi, G.; Franzò, G.; Iacona, F.; Boninelli, S.; Miritello, M.; Cesca, T.; Priolo, F.  $\text{Eu}^{3+}$  reduction and efficient light emission in  $\text{Eu}_2\text{O}_3$  films deposited on Si substrates. *Opt. Express* **2012**, *20*, 5501–5507. [[CrossRef](#)] [[PubMed](#)]
8. Burmester, P.; Ishii, T.; Huber, G.; Kurfiss, M.; Schilling, M. Characterization of crystalline europium doped  $\alpha\text{-Y}_2\text{O}_3$  PLD-films grown on  $\alpha\text{-Al}_2\text{O}_3$ . *Mater. Sci. Eng. B* **2003**, *105*, 25–29. [[CrossRef](#)]
9. Gün, T.; Kahn, A.; İleri, B.; Petermann, K.; Huber, G. Two-dimensional growth of lattice matched Nd-doped  $(\text{Gd}, \text{Lu})_2\text{O}_3$  films on  $\text{Y}_2\text{O}_3$  by pulsed laser deposition. *Appl. Phys. Lett.* **2008**, *93*, 053108. [[CrossRef](#)]
10. Babayevskaya, N.; Kryzhanovskaya, A.; Matveevskaya, N.; Mateichenko, P.; Yavetskiy, R.; Tolmachev, A.; Tret'yak, S. Composite phosphor films based on spherical  $\text{Lu}_2\text{O}_3$ :  $\text{Eu}^{3+}$  nanoparticles. *Tech. Phys. Lett.* **2011**, *37*, 174–177. [[CrossRef](#)]
11. Babayevskaya, N.; Bezkrovnyi, A.; Mateychenko, P.; Vovk, O.; Yavetskiy, R. Sol-gel processing of transparent  $\text{Lu}_2\text{O}_3$ :  $\text{Eu}^{3+}$  phosphor films. *Funct. Mater.* **2010**, *17*, 537–542.
12. Popielarski, P.; Paprocki, K.; Bala, W.; Banaszak-Piechowska, A.; Walczyk, K.; Fabisiak, K.; Szybowicz, M. Raman and impedance spectroscopy of blend polycarbonate and zinc oxide layers grown by sol-gel method. In Proceedings of the Solid State Phenomena, Lviv, Ukraine, 3–7 September 2012; pp. 22–26.
13. Bala, W.; Zorenko, Y.; Savchyn, V.; Voznyak, T.; Paprocki, K.; Popielarski, P.; Szybowicz, M. Optical and electrical properties of ZnO thin films grown by sol-gel method. In Proceedings of the Solid State Phenomena, Lviv, Ukraine, 3–7 September 2012; pp. 14–21.
14. Frackowiak, S.; Zych, E.; Kozłowski, M.; Kepinski, L. Modifying the luminescence characteristics of  $\text{Lu}_2\text{O}_3$ : Eu large nanocrystals with polycarbonate host. *Polym. Compos.* **2016**, *37*, 1330–1334. [[CrossRef](#)]
15. Meltzer, R.; Feofilov, S.; Tissue, B.; Yuan, H. Dependence of fluorescence lifetimes of  $\text{Y}_2\text{O}_3$ :  $\text{Eu}^{3+}$  nanoparticles on the surrounding medium. *Phys. Rev. B* **1999**, *60*, R14012. [[CrossRef](#)]
16. Meltzer, R.; Yen, W.; Zheng, H.; Feofilov, S.; Dejneka, M.; Tissue, B.; Yuan, H. Interaction of rare earth ions doped in nanocrystals embedded in amorphous matrices with two-level systems of the matrix. *J. Lumin.* **2001**, *94*, 221–224. [[CrossRef](#)]
17. Vetrone, F.; Boyer, J.-C.; Capobianco, J.A.; Speghini, A.; Bettinelli, M. A spectroscopic investigation of trivalent lanthanide doped  $\text{Y}_2\text{O}_3$  nanocrystals. *Nanotechnology* **2003**, *15*, 75. [[CrossRef](#)]
18. Hreniak, D.; Gluchowski, P.; Strek, W.; Bettinelli, M.; Kozłowska, A.; Kozłowski, M. Preparation and upconversion properties of  $\text{Er}^{3+}$ ,  $\text{Yb}^{3+}$ :  $\text{Y}_2\text{Si}_2\text{O}_7$  nanocrystallites embedded in PVA polymer nanocomposites. *Mater. Sci. Wroc.* **2006**, *24*, 405.
19. Trojan-Piegza, J.; Zych, E.; Hreniak, D.; Stręk, W.; Kępiński, L. Structural and spectroscopic characterization of  $\text{Lu}_2\text{O}_3$ : Eu nanocrystalline spherical particles. *J. Phys. Condens. Matter* **2004**, *16*, 6983. [[CrossRef](#)]

20. de Mello Donegá, C.; Meijerink, A.; Blasse, G. Saturation effects in the excitation spectra of rare-earth ions. *J. Lumin.* **1994**, *62*, 189–201. [[CrossRef](#)]
21. Dorenbos, P. Relation between  $\text{Eu}^{2+}$  and  $\text{Ce}^{3+}$   $f \leftrightarrow d$ -transition energies in inorganic compounds. *J. Phys. Condens. Matter* **2003**, *15*, 4797. [[CrossRef](#)]
22. Dorenbos, P. A review on how lanthanide impurity levels change with chemistry and structure of inorganic compounds. *ECS J. Solid State Sci. Technol.* **2013**, *2*, R3001–R3011. [[CrossRef](#)]
23. Dorenbos, P. Charge transfer bands in optical materials and related defect level location. *Opt. Mater.* **2017**, *69*, 8–22. [[CrossRef](#)]
24. Trojan-Piegza, J.; Zych, E. Afterglow luminescence of  $\text{Lu}_2\text{O}_3$ : Eu ceramics synthesized at different atmospheres. *J. Phys. Chem. C* **2010**, *114*, 4215–4220. [[CrossRef](#)]
25. Trojan-Piegza, J.; Niittykoski, J.; Hölsä, J.; Zych, E. Thermoluminescence and kinetics of persistent luminescence of vacuum-sintered  $\text{Tb}^{3+}$ -doped and  $\text{Tb}^{3+}$ ,  $\text{Ca}^{2+}$ -codoped  $\text{Lu}_2\text{O}_3$  materials. *Chem. Mater.* **2008**, *20*, 2252–2261. [[CrossRef](#)]
26. Trojan-Piegza, J.; Zych, E.; Hölsä, J.; Niittykoski, J. Spectroscopic properties of persistent luminescence phosphors:  $\text{Lu}_2\text{O}_3$ :  $\text{Tb}^{3+}$ ,  $\text{M}^{2+}$  ( $\text{M} = \text{Ca}, \text{Sr}, \text{Ba}$ ). *J. Phys. Chem. C* **2009**, *113*, 20493–20498. [[CrossRef](#)]
27. Kulesza, D.; Bolek, P.; Bos, A.J.; Zych, E.  $\text{Lu}_2\text{O}_3$ -based storage phosphors. An (in) harmonious family. *Coord. Chem. Rev.* **2016**, *325*, 29–40. [[CrossRef](#)]



© 2019 by the authors. Licensee MDPI, Basel, Switzerland. This article is an open access article distributed under the terms and conditions of the Creative Commons Attribution (CC BY) license (<http://creativecommons.org/licenses/by/4.0/>).